

On the possible core shift break in relativistic jets

E. E. Nokhrina^{1*}

¹*Lebedev Physical Institute, Leninsky prosp. 53, Moscow, 119991, Russia*

Accepted 2024 November 5. Received 2024 November 5; in original form 2024 June 23

ABSTRACT

Measurement of a jet geometry transition region is an important instrument of assessing the jet ambient medium properties, plasma bulk motion acceleration, parameters of a black hole and location of a jet launching radius. In this work we explore the possibility of a presence of a core shift break, associated with the geometry and jet physical properties transition. We obtain the relations on the core shift offset jump due to a change in a core shift exponent. The condition of a proper frame magnetic field continuity and the core shift break can be used as an instrument to refine the magnetic field estimates upstream the break. This method is applied to the jet in NGC 315. We speculate that the localised in a flow plasma heating either by reconnection or due to particles acceleration at the shock will also lead to a core shift break, but of a different type, than the one observed in NGC 315. We propose to use the multi-frequency core shift measurements to increase the number of sources with a detected jet shape break and to boost the accuracy of assessing the properties of a jet geometry transition region.

Key words: MHD — galaxies: active — galaxies: jets

1 INTRODUCTION

Since the first discovery of a jet shape break by [Asada & Nakamura \(2012\)](#) a lot of work has been done in order to understand the physics of this effect, and to apply it to assessing the properties of relativistic jets in active galactic nuclei (AGN). For many years jets have been thought of as a conical outflows, with the jet apparent opening angles being measured for a great number of sources (see e.g. [Pushkarev et al. 2009](#), and references within). Later the multi-epoch stacking technique has been applied to ensure the full jet width is accounted for ([Pushkarev et al. 2017](#)). Both one-epoch and multi-epoch observations revealed for the closest sources the phenomenon of a jet shape break — a transition of an observed jet boundary shape from a quasi-parabolic to a quasi-conical ([Asada & Nakamura 2012](#); [Tseng et al. 2016](#); [Hada et al. 2018](#); [Akiyama et al. 2018](#); [Nakahara et al. 2018, 2019, 2020](#); [Kovalev et al. 2020](#); [Park et al. 2021b](#); [Boccardi et al. 2021](#); [Okino et al. 2022](#)).

Jet shape on different scales may be a probe for both jet pressure at its boundary and an ambient medium pressure, and a key to understanding the FRI–FRII dichotomy. [Asada & Nakamura \(2012\)](#) discuss different models for a jet pressure, possible distributions of ambient pressure and their connection with knots HST-1 and A in M 87. [Kovalev et al. \(2020\)](#) also note the possible connection of a jet shape break

with a stationary bright feature that can be a standing shock, appearing due to a change in an ambient medium pressure profile. [Levinson & Globus \(2017\)](#), using the results by [Lyubarsky \(2009\)](#), showed, that both the observed boundary shape in M 87 jet and the position of HST-1 can be explained by introducing the abrupt change in an ambient medium pressure, although with some caveats, that they discuss. The change in an ambient medium profile is expected to occur around a Bondi radius or a radius of a sphere of gravitational influence (SGI) ([Asada & Nakamura 2012](#); [Blandford et al. 2019](#)). At the same time, most of the sources have a break at the radius $\sim 10^5 - 10^6 r_g$ ([Asada & Nakamura 2012](#); [Hada et al. 2018](#); [Kovalev et al. 2020](#)), although in the case of 1H 0323+342 the mass estimate is ambiguous ([Hada et al. 2018](#); [Nokhrina et al. 2020](#)). On the other hand, two sources with the detected jet shape break deviate from this trend. Independent evaluation of a geometry transition in NGC 315 jet by [Park et al. \(2021a\)](#); [Boccardi et al. \(2021\)](#) located the break one to two orders of magnitude in length inside the Bondi sphere. The break position in 3C 273 is detected an order of magnitude outside the SGI ([Okino et al. 2022](#)). These sources require disk winds, torus or hot cocoon surrounding a jet ([Bromberg et al. 2011](#)) to account for a change in an ambient medium pressure profile that can lead to a jet shape break.

The connection between a transition from a quasi-parabolic to a quasi-conical jet boundary shape and a plasma acceleration profile has been proposed by [Lyubarsky](#)

* E-mail: nokhrinaelena@gmail.com

(2009); Hada et al. (2018); Kovalev et al. (2020). Analytical solution by Lyubarsky (2009) predicted such a transition when the flow becomes particle-dominated. In fact, Komissarov et al. (2007) using numerical simulations noted the smooth evolution of a pressure profile at the jet boundary. Beskin et al. (2017); Kovalev et al. (2020) obtained the change in a jet pressure and the corresponding change in a jet boundary shape as the flow accelerates up to half of maximum Lorentz factor. As it was shown by Tomimatsu & Takahashi (2003); Beskin & Nokhrina (2006); Komissarov et al. (2007); Lyubarsky (2009); Tchekhovskoy et al. (2009), a jet accelerates with the bulk Lorentz factor of plasma motion Γ growing almost linearly with the jet width d as

$$\Gamma \approx \frac{d/2}{R_L}. \quad (1)$$

Here the light cylinder radius $R_L = c/\Omega_F$ is defined by the angular velocity Ω_F constant at least in the inner part of a jet (Lyubarsky 2009). After reaching the value $\Gamma_{\max}/2$, Lorentz factor growth saturates and becomes logarithmically slow (Beskin & Nokhrina 2006). Γ_{\max} corresponds to the maximum bulk motion Lorentz factor if all the electromagnetic energy is transformed into plasma kinetic energy. Depending on the normalisation, it is proportional to the jet initial magnetisation σ_M with a factor of a few (Beskin & Nokhrina 2006; Nokhrina et al. 2020). The pressure on a jet boundary is different for a magnetically dominated and plasma dominated regimes (Vlahakis 2004; Nokhrina & Pushkarev 2024). Thus, the single ambient medium pressure power law dependence on a distance along a jet, consistent with Bondi accretion, can account for the break in a jet shape. The connection between this break and an acceleration saturation has been explored by Hada et al. (2018); Nakamura et al. (2018); Kovalev et al. (2020); Ricci et al. (2022). This connection allows estimating such properties of a jet as a light cylinder radius and ambient medium pressure amplitude (Nokhrina et al. 2020).

The transformation of a Poynting flux into plasma bulk motion kinetic energy flux is not the only structural change of a jet that influences its pressure at the boundary. The appearance of a dense core with almost uniform plasma density and a poloidal magnetic field has been predicted for high enough ambient pressure, expected on the sub-parsec scales (Komissarov et al. 2009; Beskin & Nokhrina 2009). The change in a jet pressure connected with this transformation leads to appearance of an inner break and has been confirmed in M 87 jet on the scales of the order of a few milliarcseconds from the jet base (Beskin et al. 2024).

Extrapolating the boundary field line down to the gravitational radius scale may provide an answer to a jet origin: Asada & Nakamura (2012); Nakamura et al. (2018); Nokhrina et al. (2022) argue that the jet in M 87 is launched from the regions nearby the central black hole, suggesting that the main jet power is a Blandford–Znajek process (Blandford & Znajek 1977). It is worth noting that to do this, it is important to fit not only the power of jet shape on small scales, but also the position of an apex of fitted quasi-parabola (Hada et al. 2011; Kovalev et al. 2020).

There are limitations on detecting the phenomenon of a jet shape break directly due to the finite resolution of existing instruments. Indeed, jet shape break has been observed

directly only for a dozen nearby sources (typical red shift of the order of a few tenth or less), and those observed at relatively large viewing angles (for example, for BL Lac the viewing angle $\theta = 7^\circ.6$). The last fact is connected with the resolution along a jet. Due to the same issue, the breaks has been observed up to now, probably, mainly in jets with large enough light cylinder radius. Indeed, if the break is explained by a conversion of a half of a Poynting flux into a plasma bulk motion kinetic energy flux, then, for the observed maximum Lorentz factors $\lesssim 50$ (Lister et al. 2019), the jet width at the break is of the order of $100 - 200R_L$. The cited above works provide the observed jet width at the break to be of the order of a few tenths of a parsec, which leads to rather large light cylinder radii $\sim 10^{-3}$ pc (Nokhrina et al. 2019, 2020). The corresponding estimate of a light cylinder radius for the jet in M 87 was confirmed independently by modelling analytically the kinematics by Kino et al. (2022). Up to now only the jet in NGC 315 has been resolved so finely, that the implied dimensionless black hole spin is close to unity, which means that the light cylinder radius constitutes a few gravitational radii (Ricci et al. 2022). All these circumstances pose limitations on studying the jet shape break phenomenon directly on a larger sample of sources.

There can be an indirect way to detect the effect in more distant jets or jets, observed at smaller observational angles. It was shown that the plasma bulk Lorentz factor, estimated by the delays in flares from radio cores at 8 and 15 GHz (Kudryavtseva et al. 2011; Kutkin et al. 2019) and the position of these cores, obtained using core shift method, are consistent with a parabolic jet shape for the sources with red shifts up to ~ 2 (Nokhrina et al. 2022). However, this method requires multi-epoch observations, high variability of a source and do not provide directly the position of a break.

We discuss here the possibility of detecting a jet shape break allowed that it is also seen as a break in an apparent (projected) core position r_{core} as a function of observational frequency ν . First of all, there are now many indications, that the core shift exponent k_r in the dependence

$$r_{\text{core}} = \Omega_{r\nu} \nu^{-1/k_r}, \quad (2)$$

can deviate from the unity, expected in conical non-accelerating jets (see e.g., Nokhrina et al. 2022, and the references within). Here $\Omega_{r\nu}$ is a core shift offset, which depends on the physical properties affecting the synchrotron opacity at the core. As the dependence of an apparent core shift on the observational frequency is different for different flow regimes (magnetically/plasma dominated) and for different observed boundary shapes (Nokhrina et al. 2022; Ricci et al. 2022; Nokhrina & Pushkarev 2024), one may expect to detect its break. We explore this possibility in this paper. We use the results from the papers Ricci et al. (2022) and Nokhrina & Pushkarev (2024) and refer to them as R22 and N24 for brevity everywhere below.

The paper is organised as follows. In section 2 we develop the theoretical basis and discuss the break in a core shift offset. Assuming the magnetic field continuity, we obtain the formulas that can be applied to the particular sources in section 3. We show the results for NGC 315 in section 4. Finally, we discuss the results and possible appli-

cations of a method in 5 and summarise our work in section 6.

2 BREAK IN A CORE SHIFT

In general, a jet can be divided in three regions depending on its local shape: quasi-parabolic, quasi-conical and more or less smooth transition between them. In this work we regard for simplicity two asymptotic power laws (parabolic and conical). We extrapolate them into a transition region, so they intersect at the distance r_{br} . Thus, we model the jet boundary shape by the function

$$d = d_{\text{br}} \left(\frac{r}{r_{\text{br}}} \right)^k, \quad k = \begin{cases} k_1, & r \leq r_{\text{br}}, \\ k_2, & r > r_{\text{br}}, \end{cases} \quad (3)$$

where d is the jet width at the distance r along a jet, and k is an exponent that defines the particular boundary shape. Upstream the break an outflow sustains a quasi-parabolic shape with $k_1 \approx 0.5$, while downstream an exponent $k_2 \approx 1$ corresponds to a quasi-conical flow. Here and below r is a distance from the jet base. For the radio core given by Equation (2) $r = 0$ corresponds to the infinite observational frequency.

The bulk plasma motion Lorentz factor Γ affects the magnitudes of an emitting plasma number density and a magnetic field in a plasma proper frame. Magnetohydrodynamical modelling provides three distinct phases of its growth: the effective acceleration given by Equation (1), the transitional domain, where the acceleration slows down, and the saturation domain, where the bulk Lorentz factor grows logarithmically slow with a distance (Tomimatsu & Takahashi 2003; Beskin & Nokhrina 2006; Komissarov et al. 2009; Lyubarsky 2009; Tchekhovskoy et al. 2009). We connect the jet boundary shape with the Lorentz factor behaviour (Beskin et al. 2017; Nokhrina et al. 2019; Kovalev et al. 2020; Ricci et al. 2022). Assuming for simplicity two asymptotic domains, we set the following dependence of a maximum bulk Lorentz factor on a local jet width d for a given jet cross-cut:

$$\Gamma = \begin{cases} \rho \frac{d}{2R_L}, & d \leq d_{\text{br}}, \\ \frac{\Gamma_{\text{max}}}{2}, & d > d_{\text{br}}. \end{cases} \quad (4)$$

In the region $r \leq r_{\text{br}}$ ($d \leq d_{\text{br}}$) a jet is dominated by the Poynting flux and effectively accelerates. The coefficient ρ defines how strongly the Lorentz factor of a bulk plasma motion deviates from the ideal linear acceleration given by Equation (1). It accounts for both a transition between acceleration and saturation domains and a possible presence of a slow sheath. Typical values of ρ from analytical and numerical simulations are 0.20 – 0.55 (Komissarov et al. 2007; Chatterjee et al. 2019; Beskin et al. 2017; Kovalev et al. 2020). Further downstream we assume that an outflow is dominated by a plasma bulk motion kinetic energy flux, an acceleration saturates, and a jet assumes a quasi-conical shape, described by the Equation (3), with $k_2 = 1$ for a strict cone. Here we must emphasize that the detected break in a jet shape does not necessarily coincides with the boundary between the Poynting – kinetic energy flux dominance (see

e.g. Figure 7 in Kovalev et al. (2020)). However, we assume that both are located in the transition region. As we regard two asymptotic branches, we set r_{br} and d_{br} to represent both a break in a jet shape and a flow transition from effective to saturated acceleration. We denote all the values upstream the break in a core shift with an index “1”, downstream — with an index “2”, and in a plasma proper frame — with an asterisk.

We assume the power law dependencies of physical quantities that define synchrotron opacity on a jet width d or, equally, on a distance along a jet r . A dominant magnetic field B_* and an emitting plasma number density amplitude K_{e*} in a plasma proper frame are defined by the expressions

$$B_* = B_{* \text{br}} \left(\frac{r_{\text{br}}}{r} \right)^{k_b}, \quad k_b = \begin{cases} k_{b1}, & r \leq r_{\text{br}}, \\ k_{b2}, & r > r_{\text{br}}, \end{cases} \quad (5)$$

and

$$K_{e*} = K_{e* \text{br}} \left(\frac{r_{\text{br}}}{r} \right)^{k_n}, \quad k_n = \begin{cases} k_{n1}, & r \leq r_{\text{br}}, \\ k_{n2}, & r > r_{\text{br}}. \end{cases} \quad (6)$$

Here the exponents k_n and k_b may in general change at the r_{br} . We fix the values of a magnetic field and an emitting plasma number density amplitude at the distance r_{br} as $B_{* \text{br}}$ and $K_{e* \text{br}}$ correspondingly. The emitting plasma number density has an energy distribution $dn_* = K_{e*} \gamma^{-1-2\alpha} d\gamma$, $\gamma \in [\gamma_{\text{min}}, \gamma_{\text{max}}]$, with an exponent defined by the spectral index α in an optically thin regime. It is related to its amplitude K_{e*} by the standard expression $n_* \approx K_{e*} / 2\alpha \gamma_{\text{min}}^{2\alpha}$. We set the broken power law dependence of a Doppler factor

$$\delta = D \left(\frac{r}{r_{\text{br}}} \right)^{k_\delta} \quad (7)$$

with $k_{\delta 1} \neq k_{\delta 2}$ in general. For the observational angle $\theta < \Gamma_{\text{max}}$ one can set $\delta(r) \approx 2\Gamma(r)$, so that

$$\delta = \Gamma_{\text{max}} \left(\frac{r}{r_{\text{br}}} \right)^{k_\delta}, \quad k_\delta = \begin{cases} k, & r \leq r_{\text{br}}, \\ 0, & r > r_{\text{br}}. \end{cases} \quad (8)$$

If a jet is observed at the angle larger than Γ_{max} , we detect predominantly the slower parts of an outflow with $\Gamma \lesssim \theta^{-1}$. In this case one can set $\delta = \text{const}$ everywhere along a jet.

Equations (3)–(8) provide the projected position r_{core} of a radio core — a surface where an optical depth is equal to unity — to be a power law function of an observational frequency ν given by the Equation (2) with

$$k_r = \frac{k_n + (1.5 + \alpha)(k_b - k_\delta) - k}{2.5 + \alpha}. \quad (9)$$

The Equation (2) holds in two separate domains, where $d(r)$, $\Gamma(r)$, $B_*(r)$, $K_{e*}(r)$ and $\delta(r)$ can be described by a single power law.

It follows from the plasma number density flux continuity that in the effective acceleration regime (the first line of the Equation (4)) $k_{n1} = 3k$, while in the saturation regime (the second line of the Equation (4)) $k_{n2} = 2k$ (see details in R22 and N24). In the effective acceleration domain the plasma proper frame magnetic field is either dominated by the poloidal component or the latter is of the same order as the toroidal component (Vlahakis 2004; Komissarov et al. 2007). In the saturation domain the toroidal component dominates in the plasma proper frame. Thus, we use $k_{b1} = 2k$ and $k_{b2} = k$ correspondingly. In particular, for a conical jet boundary geometry with $k = 1$, $k_{n2} = 2$, $k_{b2} = 1$

and $k_\delta = 0$ in accordance with Blandford & Königl (1979). The described above differences in the exponents affect the values of the core shift exponent k_r in the Equation (9). In a plasma-dominated regime $k_{r2} = k_2$ (R22). In a Poynting-dominated domain the core shift exponent $k_{r1} = 2k_1$ if a jet is observed at a viewing angle $\theta \approx \Gamma^{-1}$ (Doppler factor $\delta \approx \text{const}$, see N24). For a smaller viewing angle $\theta \ll \Gamma^{-1}$ ($\delta \approx 2\Gamma$) the core-shift exponent is defined by the expression $k_{r1} = k_1(3.5 + \alpha)/(2.5 + \alpha)$.

Measuring in milliarcseconds the shift Δr_{mas} between the core positions at two different observational frequencies ν_1 and ν_2 , we calculate the core shift offset (Lobanov 1998)

$$\Omega_{r\nu} = 4.85 \times 10^{-9} \frac{\Delta r_{\text{mas}} D_L}{(1+z)^2} \left(\frac{\nu_1^{1/k_r} \nu_2^{1/k_r}}{\nu_2^{1/k_r} - \nu_1^{1/k_r}} \right) \text{ pc GHz}^{1/k_r}. \quad (10)$$

Here a source is located at the luminosity distance D_L and corresponding cosmological red shift z . On the other hand, the modelling shows that a core shift offset depends on a jet geometry and its physical properties (Lobanov 1998; Hirotani 2005; Nokhrina & Pushkarev 2024):

$$\left(\frac{\Omega_{r\nu}}{\sin \theta} \right)^p = \frac{C(\alpha) d_{\text{br}}}{\sin \theta} \left(\frac{D}{1+z} \right)^{1.5+\alpha} r_{\text{br}}^p K_{e*} B_{*}^{1.5+\alpha}. \quad (11)$$

Here

$$p = k_n + (1.5 + \alpha)(k_b - k_\delta) - k, \quad (12)$$

and we set the reference distance for determining B_* and K_{e*} as r_{br} instead of 1 pc. Jet width d_{br} and a break position along a jet r_{br} here and below are in parsecs. The term $C(\alpha)$ is a dimensional constant, which depends on the emitting plasma energy distribution, and $C(0.5) = 580 \text{ cm}^4 (\text{s g pc})^{-1}$.

The exponents k_n , k_b , k_δ and k assume different values in different domains along a jet. We emphasize that the power law relation (2) holds only in the part of a jet, which is described by a single power law for each physical value $B_*(r)$, $K_{e*}(r)$, $\delta(r)$ and $d(r)$. This may not be a case in the transition region, where the core shift position as a function of an observational frequency changes from the one asymptotic power law to the other. We regard separately quasi-parabolic and quasi-conical domains, where the core shift exponents may differ from each other: $k_{r1} \neq k_{r2}$ (N24). The core shift offsets $\Omega_{r\nu1,2}$ can be introduced only within these regions correspondingly. In general, $\Omega_{r\nu1} \neq \Omega_{r\nu2}$, and it is to this difference in two physically and geometrically different jet domains we refer as a ‘break in a core shift offset’. The two branches described by the Equation (2) can also be extrapolated onto the region of a smooth transition: see, for example, the upper panel in Figure 1.

Let us discuss different possibilities of a jet boundary shape break and its impact on the value of the core shift offset. Equation (11) shows that if there is no discontinuities in a jet properties (velocity, emitting plasma number density and magnetic field), than a core shift offset may assume different values in two distinct region only if $p_1 \neq p_2$. From the Equations (9) and (12) we obtain that $k_{r1} \neq k_{r2}$ either. Then, for any acceleration regime, Equation (11) provides the jump in a core shift offset for two asymptotic domains,

and its value is given by

$$\begin{aligned} \frac{\Omega_{r\nu1}}{\Omega_{r\nu2}} &= \left(\frac{\Omega_{r\nu2}}{r_{\text{br}} \sin \theta} \right)^{(k_{r2}/k_{r1}-1)} = \\ &= \left(\frac{\Omega_{r\nu1}}{r_{\text{br}} \sin \theta} \right)^{(1-k_{r1}/k_{r2})}. \end{aligned} \quad (13)$$

There can be several different physical cases underlying such a jump.

Pure jet shape change within one of the regimes of plasma acceleration. Suppose the jet changes its shape at the distance r_{br} due to a change in an ambient medium pressure, i.e. $k_1 \neq k_2$. However, the plasma acceleration regime is the same: either effective or saturated acceleration. The powers k_n , k_b , k_δ are different in the regions $r < r_{\text{br}}$ and $r > r_{\text{br}}$, as the physical values depend on a jet width $d(r)$. Consequently, k_r and p change, leading to two different power laws with different core shift offsets.

Pure change of acceleration regime without a jet shape change. Although $k_1 = k_2$ in this case, the exponents k_n , k_b , k_δ change as the outflow transits from Poynting to kinetic energy flux dominance. The exponents k_r and p are also different, and $\Omega_{r\nu1} \neq \Omega_{r\nu2}$.

Jet changes its shape and plasma acceleration regime simultaneously. In the case of $\theta \ll \Gamma^{-1}$ ($\delta \approx 2\Gamma$, see Equation (25) in N24) the powers k_r are, in general, not equal to each other even for ideal situation $k_1 = 0.5$, $k_2 = 1$: $k_{r1} = 4k_1/3 \approx 0.66$ and $k_{r2} = k_2 \approx 1$. Thus, the jump in core shift offset is always present in this case.

Suppose the core shift exponents have approximately equal values. This can take place for a jet observed at large enough viewing angle, so that we can set Doppler factor to be approximately constant. In the ideal situation $k_1 = 0.5$, $k_2 = 1$, $k_{r1} = 2k_1$ and $k_{r2} = k_2$. In this case the equality $k_{r1} \approx k_{r2}$ holds, and the jump in core shift offset is absent: although such physical values as emitting plasma number density and magnetic field have different dependencies on r in two different regions, both branches of a core shift coincide, ensuring the same value of $\Omega_{r\nu1} = \Omega_{r\nu2}$ along a jet.

In Figure 1 we present the cartoon of possible asymptotic core shift branches behaviour. In general, we expect $k_{r1} \leq k_{r2}$ for a flow that is better collimated at its base. The upper panel demonstrates the case of NGC 315, in which two asymptotic branches intersects, which holds while $\Omega_{r\nu1} > \Omega_{r\nu2}$. We do not exclude the opposite case $\Omega_{r\nu1} < \Omega_{r\nu2}$, presented in the medium panel. Here we predict two non-intersecting branches.

Case of a jump in plasma properties. Suppose now that neither a jet shape nor plasma acceleration regime changes, so the core shift exponent k_r is the same everywhere. However, there is a jump in emitting plasma number density K_{e*} and magnetic field B_* . This can be a consequence of either a plasma heating or a propagating flare. In general, the jump in core shift offset in this case is equal to

$$\frac{\Omega_{r\nu1}}{\Omega_{r\nu2}} = \left(\frac{K_{e*1} B_{*1}^{1.5+\alpha}}{K_{e*2} B_{*2}^{1.5+\alpha}} \right)^{1/p}. \quad (14)$$

Example of such a core shift break is presented in Figure 1, the lower panel. In this case the core shift exponents are the same, but the jump in the offset is due to abruptly changed balance between a magnetic field and an emitting plasma energy densities.

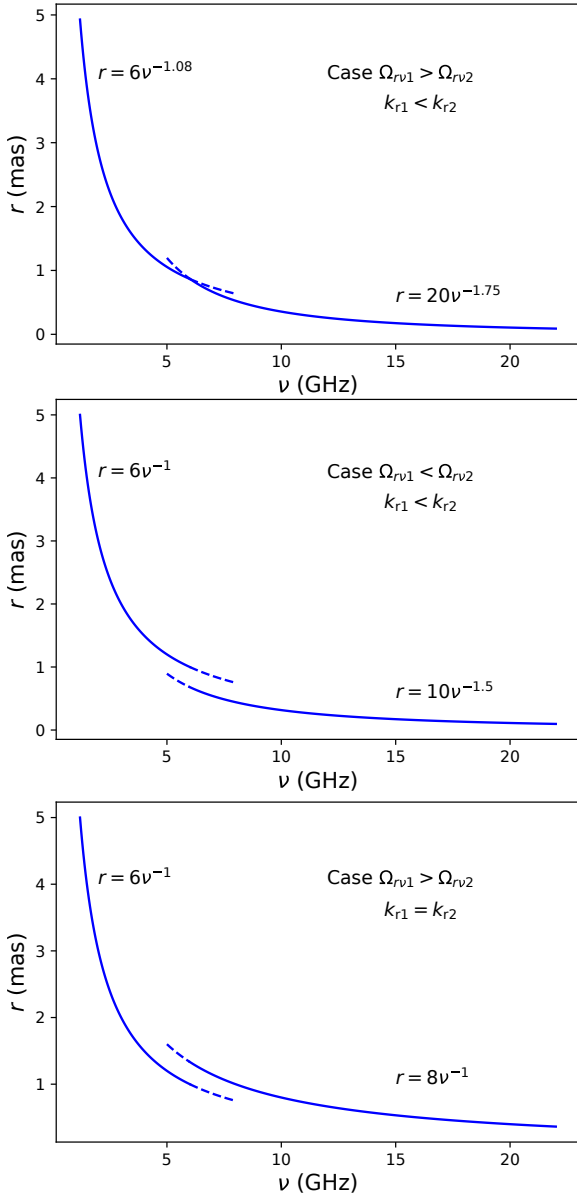


Figure 1. Cartoons of the possible scenarios of a core shift break. Upper panel: case of $\Omega_{r\nu 1} > \Omega_{r\nu 2}$ and $k_{r1} < k_{r2}$ as observed in NGC 315. Medium panel: case of $\Omega_{r\nu 1} = \Omega_{r\nu 2}$ or $\Omega_{r\nu 1} < \Omega_{r\nu 2}$ and $k_{r1} < k_{r2}$. Lower panel: case of $\Omega_{r\nu 1} > \Omega_{r\nu 2}$ and $k_{r1} = k_{r2}$, possible for a jump in K_{e*} and B_* . Extrapolation of each branch onto adjacent region is shown in dashed lines. Here r is measured from the jet base, assuming its coincidence with the radio core position at infinite frequency.

The jump in a core shift offset must be expected in jets. For the continuous flow properties its presence is a consequence of different values of a core shift exponent k_r in different regions of a jet. If it is caused by the jet shape and / or acceleration regime break, its value is universally described by Equation (13). In this case we cannot distinguish whether a jump in a core shift offset is present because of a change in a plasma acceleration pattern or because of a change in a jet shape due to different properties of a collimating medium. If the jump in a core shift offset is due to a change in emitting plasma number density / magnetic

field (see Equation (14)), than we expect the same value of the exponent k_r . The value of the jump, in general, would not obey the Equation (13), which allows distinguishing the possible effect of a flaring event on a core shift.

3 MATCHING MAGNETIC FIELD AT THE BREAK

Let us assume that the multi-frequency measurements of a core shift are consistent with a break in the Equation (2) at some break frequency ν_{br} . In particular, suppose that we measure k_{r1} for $\nu > \nu_{br}$ and k_{r2} for $\nu < \nu_{br}$. In this case there is in general a jump in the core shift offset as well. Below we regard the simultaneous change in both the plasma acceleration regime and in jet boundary shape as a cause.

The corresponding $\Omega_{r\nu 1}$ and $\Omega_{r\nu 2}$ can be calculated using the observational data in two separate jet parts. Correspondingly, the frequencies, between which one can calculate the core shift offset, are divided in two sets: for the cores situated in one asymptotic region, and in the other. Mixing the frequencies may lead to unreliable results for the core shift offset. From each set of observational frequencies and the definition given by the Equation (2) we readily obtain the de-projected position of an expected jet shape break in parsecs as

$$r_{br} = \frac{\Omega_{r\nu 1}}{\nu_{br}^{1/k_{r1}} \sin \theta}. \quad (15)$$

Here ν_{br} is in GHz and $\Omega_{r\nu 1}$ is in $\text{pc GHz}^{1/k_{r1}}$. If the apparent opening angle $\varphi_{app} = 2\varphi / \sin \theta$ is measured at the frequencies $\nu > \nu_{br}$ (the expected conical part of a jet), one can use the expression

$$d_{br} = \varphi_{app} \frac{\Omega_{r\nu 1}}{\nu_{br}^{1/k_{r1}}} \quad (16)$$

as a proxy for a jet width at the break. Both estimates given by Equations (15) and (16) may be approximate if the intersection of two branches of a core shift do not coincide precisely with the jet geometry transition distance r_{br} .

Having two branches of the measured core shift, corresponding to two different jet boundary shapes, one can match the corresponding magnetic fields, calculated in two different regions.

Suppose first, that the break in a core shift dependence on the frequency has been detected together with a break in a jet shape. In this case we have the following set of measured parameters: the position of a break along a jet r_{br} , the jet width at the break d_{br} , jet shape exponents k_1 in a quasi-parabolic domain and k_2 in a quasi-conical domain, k_{r1} and k_{r2} — corresponding powers in Equation (2), $\Omega_{r\nu 1}$ and $\Omega_{r\nu 2}$ — core shift offsets in two domains. Let us obtain the conditions, under which the estimates for the magnetic field at the break from the conical and parabolic domains are equal to each other.

Consider the case of a constant Doppler factor in both accelerating and saturation regions. Equating RHS of the Equation (23) by N24 and Equation (12) by R22, we get the relation

$$\frac{\eta \Gamma_{max}}{\rho^2} = 0.045 \frac{\Omega_{r\nu 1}^{p_1}}{\Omega_{r\nu 2}^{p_2}} (r_{br} \sin \theta)^{p_2 - p_1} \quad (17)$$

that ensures the continuity of a magnetic field in a plasma proper frame in parabolic (Poynting dominated) and conical (plasma bulk kinetic energy dominated) domains. Here η is a fraction of emitting plasma (see details in N24). Equation (17) improves assessment of a magnetic field strength by fixing the value of $\eta\Gamma_{\max}/\rho^2$ term.

Suppose now, that only the break in a core shift dependence on the frequency has been obtained, while the break in a jet form has been undetected due to the resolution reasons. In this case we presume that $k_1 = k_{r1}/2$ and $k_2 = k_{r2}$ (see details in R22 and N24). The position of a break is approximated by Equation (15). In this case we obtain

$$\frac{\eta\Gamma_{\max}}{\rho^2} = 0.045 \left(\frac{\Omega_{r\nu1}}{\Omega_{r\nu2}} \right)^{(2.5+\alpha)k_{r2}} \nu_{\text{br}}^{(2.5+\alpha)(1-k_{r2}/k_{r1})}. \quad (18)$$

Together with a break position assessment by Equations (15) and (16) it again improves the magnetic field estimate.

For the case of a small enough viewing angle, when the Doppler factor in an accelerating domain depends on a Lorentz factor as $\delta \approx 2\Gamma$, we equate the magnetic field from Equations (25) by N24 and (29) (in Equation (25) there is a misprint, ρ^2 should be absent):

$$\frac{\eta\Gamma_{\max}d_{\text{br}}^2}{R_L^2} = 0.045\delta^2 \frac{\Omega_{r\nu1}^{p_1}}{\Omega_{r\nu2}^{p_2}} (r_{\text{br}} \sin \theta)^{p_2-p_1}, \quad (19)$$

where δ is a Doppler factor in the saturation domain. Hence, one can set $\delta = \Gamma_{\max}$. Using the relation (4), we obtain exactly the Equation (17), although the exponent p_1 in this case is different due to non-zero k_δ (see Equation (12)). Again, if the jet boundary shape has not been measured, the condition on the value of a parameter $\eta\Gamma_{\max}/\rho^2$ is given by Equation (18).

Thus, matching the magnetic field at the jet shape geometry transition point restricts the model parameters with the universal Equations (17) and (18) and allows for the more precise magnetic field estimate. Only the parabolic branch allows to extrapolate the magnetic field upstream the break. Simple extrapolation of B_* calculated in the conical region into parabolic part of a jet may provide incorrect result.

4 MAGNETIC FIELD IN NGC 315

A jet from the source NGC 315 is unique, since both a break in a jet boundary shape and a break in frequency dependence of a core shift have been located by [Boccardi et al. \(2021\)](#) and [Ricci et al. \(2022\)](#). Here we present the study of a magnetic field structure in NGC 315 jet using these results.

Let us assume that we observe a jet in NGC 315 at the viewing angle $\theta \approx \Gamma^{-1}$ (the Doppler factor $\delta \approx \text{const}$). We use the exponent $k_{r1} = 0.57 \pm 0.17$ (R22) and the core shifts between ten pairs of frequencies 43.2, 22.3, 15.4, 12.1, 8.4 GHz ([Boccardi et al. 2021](#)) in quasi-parabolic domain. In quasi-conical region we use $k_{r2} = 0.93 \pm 0.01$ and three pairs of frequencies 8.4, 5.0, 1.4 GHz. The corresponding core shift offsets are equal to $\Omega_{r\nu1} = 13.2 \pm 5.3 \text{ pc GHz}^{1.75}$ and $\Omega_{r\nu2} = 2.58 \pm 0.76 \text{ pc GHz}^{1.08}$. The relation (13) holds for NGC 315 with a very good accuracy.

At first, let us check the approximations (15) and (16). Setting the break frequency $\nu_{\text{br}} = 8.4 \text{ GHz}$ (R22), we obtain $r_{\text{br}} = 0.51 \pm 0.20 \text{ pc}$, which is close to the measured

0.58 pc ([Boccardi et al. 2021](#)). On the other hand, one can reverse the expression (15) and find the break frequency, which for NGC 315 is equal to $7.8 \pm 1.8 \text{ GHz}$. Overall, the results for ν_{br} by R22 and r_{br} by [Boccardi et al. \(2021\)](#) are consistent, while the estimated r_{br} by [Park et al. \(2021a\)](#) has a value much larger than the one, obtained by using ν_{br} . For the approximation (16) we use $\varphi_{\text{app}} = 6^\circ.9$ by [Pushkarev et al. \(2017\)](#) and get $d_{\text{br}} = 0.038 \pm 0.015 \text{ pc}$. This estimate produces the value of a jet break width about two times smaller than the actual measured jet width at the break 0.072 pc ([Boccardi et al. 2021](#)). This difference may be connected with the error in estimation of apparent opening angle and with the uncertainty in the value of a viewing angle.

Using the Equation (17) we obtain the condition ensuring the equality of magnetic fields, determined within the quasi-parabolic and quasi-conical domains:

$$\frac{\eta\Gamma_{\max}}{\rho^2} = 5.25_{-4.50}^{+29.75}. \quad (20)$$

The errors in a magnetic field estimates for different sets of observational frequencies provide the errors in the relation (20). This relation does not depend on the observed Doppler factor δ , although the estimate of a magnetic field do depend on it as $\delta^{-0.5}$ (N24). Below we use $\delta = 1$ for a large observational angle $\theta = 38^\circ$ ([Boccardi et al. 2021](#)).

To calculate the magnetic field in the quasi-parabolic accelerating part of a jet in NGC 315 we use the equations (23) from N24 and Equation (12) from R22. We observe that $\Omega_{r\nu1}$ is a few times larger than $\Omega_{r\nu2}$. Even with this difference, the estimates for a magnetic field upstream and downstream the break coincide for reasonable values of a fraction of emitting plasma η , maximum Lorentz factor Γ_{\max} and coefficient ρ given by (20). Applying the condition (20), the magnetic field values in a plasma proper frame up and down the break are equal to $B_{\text{p}*, \text{br}} = 0.18 \pm 0.05 \text{ G}$ and $B_{\varphi*, \text{br}} = 0.18 \pm 0.04 \text{ G}$ correspondingly.

Let us extrapolate the magnetic field along a jet. In the domain of effective plasma acceleration one may adopt $B_* = B_{\text{p}*} = B_{\text{p}}$ ([Vlahakis 2004](#); [Komissarov et al. 2009](#)), since the plasma bulk velocity has a dominant poloidal velocity. Using the flux conservation, we obtain for $r < 0.58 \text{ pc}$ the following:

$$B_{\text{p}*}(r) = B_{\text{p}}(r) = B_{\text{p}*, \text{br}} \left(\frac{r_{\text{br}}}{r} \right)^{2k_1}, \quad r < r_{\text{br}}. \quad (21)$$

On the other hand, measured core shift in quasi-conical domain provides the toroidal magnetic field $B_{\varphi*}$ in a plasma proper frame as a dominant component. We obtain

$$B_{\varphi*}(r) = B_{\varphi*, \text{br}} \left(\frac{r_{\text{br}}}{r} \right)^{k_2}, \quad r > r_{\text{br}}. \quad (22)$$

Here $k_1 = 0.45$ is a power of a parabolic jet boundary shape $d \propto r^{k_1}$, and $k_2 = 0.84$ — of a conical shape. The results are presented in Figure 2. The corresponding magnitudes of poloidal (blue) and toroidal (green) components in a plasma proper frame are shown in solid lines. As the powers of a magnetic field dependence on distance are equal to $2k_1 = 0.9$ and $k_2 = 0.84$, the difference in slopes are hardly noticeable.

The approach of estimating magnetic field in both parabolic and conical domains allows us to assess its topology. First, the poloidal magnetic field can extrapolated

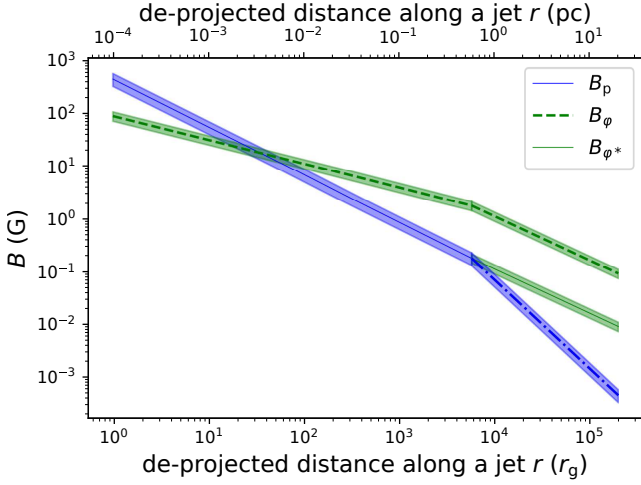


Figure 2. Blue solid line — a magnetic field poloidal component, calculated using the core shift measurements upstream the break. Shaded region shows errors. Green solid line — a magnetic field toroidal component in a plasma proper frame, calculated using the core shift measurements downstream the break. Blue dashed dotted line — extrapolation of a poloidal field downstream the break. Green dashed line — a magnetic field toroidal component recalculated into the core frame as $B_\varphi = B_{\varphi*}\Gamma_{\max}/2$. Upstream the break it was extrapolated using the dependence $B_\varphi \propto r^{-k_1}$. The toroidal magnetic field component in a plasma proper frame coincides with the poloidal component. Here we used the parameters $\Gamma_{\max} = 20$, $\rho = 0.2$, $\eta = 0.011$. Distance along the jet is de-projected with the viewing angle $\theta = 38^\circ$ (R22). A gravitational radius r_g corresponds to the black hole mass $M_{\text{BH}} = 2.08 \times 10^9 M_\odot$ (Boizelle et al. 2021).

downstream the break using the magnetic flux conservation:

$$B_p = B_{p*,\text{br}}(r_{\text{br}}/r)^{2k_2}, \quad r > r_{\text{br}} \quad (23)$$

(dashed dotted blue line in Figure 2). The proper frame toroidal field at the break $B_{\varphi*,\text{br}}$ relates to the field in a core frame $B_{\varphi,\text{br}}$ as $B_{\varphi,\text{br}} = B_{\varphi*,\text{br}}\Gamma_{\max}/2$. Here we assume that a half of an initial Poynting flux converts into the the bulk plasma motion kinetic energy flux at the break. This means $\Gamma = \Gamma_{\max}/2$, and we adopt $\Gamma_{\max} = 20$ by R22. From the break point at $r = 0.58$ pc we extrapolate B_φ upstream as

$$B_\varphi = B_{\varphi*,\text{br}} \frac{\Gamma_{\max}}{2} \left(\frac{r_{\text{br}}}{r}\right)^{k_1}, \quad r < r_{\text{br}} \quad (24)$$

and downstream as

$$B_\varphi = B_{\varphi*,\text{br}} \frac{\Gamma_{\max}}{2} \left(\frac{r_{\text{br}}}{r}\right)^{k_2}, \quad r > r_{\text{br}} \quad (25)$$

(dashed green line in Figure 2). Extrapolating $B_{\varphi*}$ upstream the break is less trivial due to changing Lorentz factor of a bulk plasma motion:

$$B_{\varphi*} = B_{\varphi*,\text{br}} \left(\frac{r_{\text{br}}}{r}\right)^{2k_1}, \quad r < r_{\text{br}}, \quad (26)$$

where it coincides with the poloidal magnetic field upstream the break. Let us note that the radio core shift is fitted by R22 with respect to the the 43 and 86 GHz radio cores, while we use the distance r from the jet base. However, this does not affect the result for a magnetic field extrapolation. The core shift offset, used to estimate $B_{*,\text{br}}$, is calculated for pairs of frequencies. Extrapolation is performed from r_{br}

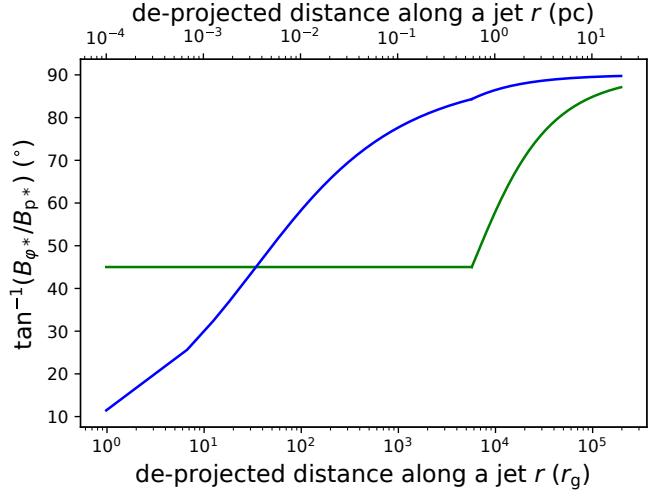


Figure 3. Angle between the magnetic field and the direction along a jet in a plasma proper frame (green line) and in a core frame (blue line). Horizontal axis is the same as in Figure 2.

obtained by the jet boundary shape modelling, which is not affected by the particular position of 43 or 86 GHz cores.

In Figure 3 we present the angle between the direction of a magnetic field and the direction of a jet in a plasma proper frame (green line). The pitch angle of emitting particles is set with respect to this angle. The blue line in Figure 3 represents an angle between a magnetic field in a core frame and a jet direction. The magnetic field topology changes from the poloidal- to the toroidal-dominated along the jet.

Now let us assume that the viewing angle $\theta \ll \Gamma^{-1}$ (the Doppler factor $\delta \approx 2\Gamma$, $k_{r1} = 4k_1/3$). Using the relation (17) or (19) with different exponent p_1 , than in the previous consideration due to $k_\delta = k$, we obtain

$$\frac{\eta\Gamma_{\max}}{\rho^2} = 0.20_{-0.17}^{+1.10}. \quad (27)$$

After ideal matching of magnetic field at the break, the picture of its distribution coincides exactly with the one, presented in Figure 2, but with amplitudes $\sqrt{\delta} = \sqrt{\Gamma_{\max}}$ times smaller.

The value $\Gamma_{\max} = 20$ is adopted from R22 (please, note, that in this paper Γ_{\max} has a different meaning and is two times smaller) as the typical one for an expected parent population. The observed values of the bulk motion Lorentz factor in NGC 315 are smaller and equal to $\sim 3-4$ (Ricci et al. 2022; Park et al. 2021a). However, for a large viewing angle, which is probably the case for NGC 315, we may not detect the fastest motion, which justifies using the greater Γ_{\max} . On the other hand, setting different maximum Lorentz factor would affect only the toroidal magnetic field in the core frame — a green dashed line in Figure 2. Using $\Gamma_{\max} \approx 8$, which provides the maximum observed $\Gamma \approx 4$, makes an estimate of a toroidal magnetic field component in a jet $2.5 = 20/8$ times smaller, while the estimates for a magnetic field in a plasma proper frame would be the same due to Equation (17).

The obtained magnetic field estimate is in a good agreement with the results in the recent work by Kino et al. (2024). Comparing the spectral index distribution with the model predictions (Ro et al. 2023), they obtained the min-

imum magnetic field at $r = 0.12$ pc ($1.6 \times 10^3 r_g$ with $M_{\text{BH}} = 1.6 \times 10^9 M_\odot$) $B = 0.8$ G, which is corroborated by the magnetic field estimate obtained above using the core shift break method. The blue solid curve in Figure 2 coincides almost exactly with the lower boundary of the grey curve in Figure 5 by Kino et al. (2024). We should emphasise the difference of the methods in the paper by Kino et al. (2024) and in this paper. Kino et al. (2024) explore the region around the break point inside the parabolic domain, where the jet bulk motion acceleration undergoes a transition phase from ideal acceleration to saturation with an approximate power law $\Gamma \sim r^{0.3}$. At the same time they estimate the toroidal magnetic field in a plasma proper frame (see e.g. Zamaninasab et al. 2014), which is of the same order with the poloidal component in the parabolic domain. Both these assumptions lead to $B_* \propto r^{-0.88}$, very close to the assumed $B_* \propto r^{-0.9}$ for $k = 0.45$ in this work. We, on the other hand, regard the domains of ideal linear acceleration and saturation, providing that core shift is measured separately between low (in conical) and high (parabolic domain) frequencies. These branches are determined for linear and saturated acceleration, but provide the result, which is close to the one obtained by Kino et al. (2024). Thus, the magnetic field behaviour, implied from studying the transition domain by Kino et al. (2024) and two far asymptotic domains in this work demonstrates a very good agreement.

We see that having measured the core shift break (R22), we are able to match the estimates of the magnetic field B_* calculated in both quasi-parabolic and quasi-conical jet domains. This is done for the reasonable, although not well restricted, values of a bulk plasma motion maximum Lorentz factor Γ_{max} and the fraction of emitting plasma η . Approximately the same results are obtained for different assumptions on a Doppler factor δ . The developed here technique refines the method proposed by N24.

5 DISCUSSION

In general, we should expect the break in an apparent core position as a function of an observational frequency. This can take place even for the continuous behaviour of a jet emitting plasma number density amplitude K_{e*} and magnetic field B_* across a break. In a case of $\delta \approx 2\Gamma$ ($k_{r1} = 4k_1/3$) the discontinuity in a core shift must be always present due to different powers in core shift in parabolic and conical regions. In a case of $\delta \approx \text{const}$, the approximate equality of $k_{r1} \approx k_{r2}$, if it happens, may wipe out the effect.

There can be two sources of a core shift break. The first one is a jump in k_r , connected with the different regimes of a jet acceleration and / or jet different shape (see the upper and medium panels in Figure 1). The second one may occur due to the jump in parameters of a jet plasma and a magnetic field as a result of a plasma heating by its acceleration on shocks or due to a reconnection (see e.g., Kirk et al. 1994; Sironi et al. 2013). These two types can be distinguished by checking the relation (13), which must hold only for the first type of a core shift offset jump. The first type of a jump in both k_r and $\Omega_{r\nu}$ due to the different regimes of a jet acceleration is observed in NGC 315 (R22), where the two branches intersect (see Figure 1, upper panel). In a case of $\Omega_{r\nu1} \leq \Omega_{r\nu2}$ it can appear as two

non-intersecting branches with different values of k_r (see Figure 1, the medium panel). The second type may appear as two non-intersecting branches as in the lower panel of the Figure 1. It is worth revisiting the multi-frequency core shift data, such as the one by (Sokolovsky et al. 2011), to search for the possible core shift breaks. We will address this issue in the upcoming paper.

The magnitudes of a poloidal and toroidal magnetic field in an AGN frame are of the same order only on the scales $d_* \sim R_L$. This corresponds to the intersection of a blue solid and green dashed lines in Figure 2. Equating the amplitudes given by equations (21) and (24) and using expression (4), we obtain the jet width $d_* = 2R_L/\rho$. Thus, for any choice of Γ_{max} the value of the light cylinder radius is self-consistent.

Measurement of both core shift and jet shape boundary break allows to refine the method of estimating a magnetic field in jets. Indeed, having the information on a core shift in both Poynting-dominated and plasma-dominated regions, we are able to limit the factor $\eta\Gamma_{\text{max}}/\rho^2$ in expressions (23) and (25) by N24 and to improve the magnetic field estimates upstream the break. Potentially, both core shift and jet shape measurements allow to fit the break simultaneously, which will increase the precision of a break location. At the same time, the localisation of a break in a core shift allows to extrapolate the magnetic field onto the gravitational radius scales correctly, assuming the total magnetic flux conservation.

Conditions (20) and (27) could be checked against the equipartition. The ratio of a magnetic to an emitting particles energy density changes along a jet for reasonable assumptions on $B_*(r)$ and $n_*(r)$ behaviour. In particular, for the dependencies (5) and (6) with $2k_b > k_n$, the emitting plasma energy density grows along the flow, which may affect the brightness temperature in the cores (Nokhrina 2017). Let us introduce the ratio of a magnetic field to an emitting plasma energy density, which is conserved along a non-accelerating jet:

$$\Sigma_\zeta = \frac{B_{*\zeta}^2}{8\pi mc^2 \Lambda K_{e*\zeta}}. \quad (28)$$

Here Λ depends on the emitting plasma energy distribution. For $\alpha = 0.5$ parameter $\Lambda = \ln(\gamma_{\text{max}}/\gamma_{\text{min}})$ and is usually set to be of the order of 10 (Lobanov 1998). With Σ_ζ and Λ explicitly written, the expression (12) from R22 for a magnetic field in a conical non-accelerating jet is modified as follows:

$$B_{*\zeta} = 0.0167 \left[\frac{\Omega_{r\nu}^2}{r_\zeta^2} \left(\frac{1+z}{\delta} \right)^{(1.5+\alpha)} \frac{\Sigma_\zeta \Lambda}{d_\zeta \sin^{p2-1} \theta} \right]^{1/(3.5+\alpha)}. \quad (29)$$

Applying this latter equality to NGC 315, we obtain for $\delta \approx \text{const}$ the relation $\Sigma_{\text{break}} \eta \Gamma_{\text{max}} / \rho^2 = 5.25_{-4.50}^{+29.75}$, which generalises the condition (20). On the other hand, combining relation (28) with the equality (22) by N24 we get

$$\frac{\Sigma_{\text{break}} \eta \Gamma_{\text{max}}}{\rho^2} = \frac{1}{\Lambda}. \quad (30)$$

For the fiducial value of the parameter $\Lambda = 10$, the generalised condition of continuity of a magnetic field in a plasma proper frame (20) is fulfilled marginally. However, the generalised condition (27) is in a good agreement with the expected values for Λ . Assuming the equipartition in conical

domain $\Sigma_{\text{break}} = 1$, we expect the equality $\eta\Gamma_{\text{max}}/\rho^2 = 0.1$. This immediately leads to the small fraction of an emitting plasma with the upper limit $\eta \leq 0.1/\Gamma_{\text{max}}$. This result is suggested by Frolova et al. (2023) basing on predicted intensity distribution. Here we must note again that the relation between an emitting plasma and magnetic field energy density (22) from N24 means, that a magnetic field dominates upstream the break. Its dominance falls as the flow propagates along a jet, and the classical equipartition holds starting from the jet shape break on. If there is no equipartition at the break, the ratio Σ_{break} still holds downstream. This can affect the measured brightness temperature of radio cores (Pjanka et al. 2017; Nokhrina 2017).

It is non-trivial, that the condition of a magnetic field continuity (27) satisfies the independent condition (30). The latter together with much better relation for a core shift exponents $k_{r1} = 4k_1/3$, may point to the non-constant Doppler factor regime in a parabolic domain (equation (25) by N24). As we noted earlier, this requires much smaller viewing angle $\theta \sim (\Gamma_{\text{max}}/2)^{-1}$ radians. Such a value of a viewing angle places the break at the distance $3.2 \text{ pc} = 3.1 \times 10^4 r_g$ for $M_{\text{BH}} = 2.08 \times 10^9 M_{\odot}$, which is still well within the estimated Bondi radius (Boccardi et al. 2021).

The method of a core shift break may provide more sources with a detected break in a jet shape, but requires the multi-frequency observations. The typical frequencies of observations are 1, 5, 8, 12, 15, 22, 43, 86 GHz, with 230 and 345 GHz available with *EHT*, *ALMA* and planning *Millimetron* programs. In order to fit the core shift dependence with the two branches, two conditions must be fulfilled.

First condition: the break frequency must be 5–12 GHz so that there are at least tree points to fit with every core shift branch. Kovalev et al. (2020); Nokhrina et al. (2020) found that a geometry transition is located at the distance $10^5 - 10^6 r_g$. On the other hand, the position as close as few of $10^3 r_g$ may be present (Boccardi et al. 2021). Below in our estimates we use the estimate $r_{\text{br}} \approx 10^4 - 10^5 r_g$. We set the typical black hole mass as $10^9 M_{\odot}$ and typical viewing angles 5° for BL Lacs and 15° for radio galaxies (see details in Kovalev et al. 2020). This places the projected distance of a jet boundary shape break at the distance 0.04–1.3 pc. Using Equation (15) with $\nu_{\text{br}} = 8 \text{ GHz}$ we obtain the lower limit for the value of a core shift offset $\Omega_{r\nu1} \gtrsim 0.9 - 9 \text{ pc GHz}^{1.5}$ for BL Lacs, and $\Omega_{r\nu1} \gtrsim 3 - 30 \text{ pc GHz}^{1.5}$ for radio galaxies, which makes the blazars preferable targets. We set here $k_r = 2/3$ for an accelerating jet with variable Doppler factor.

The second condition is a sufficient resolution at high frequencies. Assuming the typical error in core shift measurements with ground-based VLBI 0.05 mas (Sokolovsky et al. 2011; Pushkarev et al. 2012), we set the projected distance between cores at two different frequencies at $\sim 0.1 \text{ pc}$ for nearby sources. This leads to the lower limit for a core shift offset $\Omega_{r\nu1} \gtrsim 4 - 13 \text{ pc GHz}^{1.5}$ for frequency pairs 8–15 and 15–22 GHz correspondingly. The higher the observational frequency, the greater value of a core shift offset must be in order to be resolved with the ground-based interferometry. We conclude that all the nearby sources with $\Omega_{r\nu} > 1.5 \text{ pc GHz}$, calculated for $k_r = 1$ between the frequencies 8.1 and 15.4 GHz (see e.g. Pushkarev et al. 2012) (corresponding to $\Omega_{r\nu} > 5 \text{ pc GHz}^{1.5}$ for $k_r = 2/3$), may be targets for searching for the core shift break. Future *Millimetron* mission with the maximum reso-

lution $\sim 10^{-4} - 10^{-5} \text{ mas}$ (Novikov et al. 2021) will be able to easily track the jet core shift with $\Omega_{r\nu1} \sim 1 - 20$ up to the frequencies $\sim 300 \text{ GHz}$, corresponding to the planned high frequency by *EHT*. As to lower values of core shift offset, with this resolution the core shift can be measured for $\Omega_{r\nu1} \gtrsim 0.2$ at the frequency pair 86–230 GHz in nearby sources, and for $\Omega_{r\nu1} \gtrsim 1$ for the sources at red shift 1. Measuring core shifts with the ground-based VLBI at low frequencies and with *Millimetron* at high frequencies may potentially help to detect more core shift breaks in nearby sources, and collect the data for core shift dependence on the observational frequency close to a jet base even for distant sources.

It would be most beneficial to search for a core shift break in sources with already detected jet shape geometry break. However, analysis shows that the expected ν_{br} (see Equation (15)) has a value $\lesssim 1 \text{ GHz}$ for all the sources in a sample from N24, except for NGC 315 investigated here and the sources 1637+826 and 1807+698 with the break frequency expected at 3 and 4 GHz correspondingly. We do not apply the method of a core shift break to the jet in M87, since the radio cores at the observational frequencies from 230 to 5 GHz lie within the parabolic domain. However, applying the Equation (23) by N24, applicable for an accelerating flow, we obtained the results in a very good agreement with the results by Event Horizon Telescope Collaboration (2021). Again, our method provides the result in excellent agreement with Ro et al. (2023) but a few times smaller. Thus, for the sources with a detected jet shape break and expected $\nu_{\text{br}} < 1$, it is still important to conduct multi-frequency observations to study the effects of both flow acceleration and viewing angle on a core shift.

6 CONCLUSIONS

The work is dedicated to the presence of a change in core shift exponent k_r and, consequently, to the jump in a core shift offset $\Omega_{r\nu}$ at the jet geometry transition region r_{br} . As the jet changes its shape from parabolic to conical and / or plasma bulk motion acceleration — from effective to saturation regime, the opacity behaves differently in two asymptotic regions. Although the dependence of a radio core position on an observational frequency is continuous, it has two asymptotic branches, corresponding to two different k_r and $\Omega_{r\nu}$.

1. We show that, in general, the core shift offset $\Omega_{r\nu}$ must be discontinuous in the region, where the jet boundary changes its shape. In particular, it is present in the region where the plasma bulk motion pattern transits from the effective acceleration, given by the first line in Equation (4), to the extremely slow acceleration downstream. It is also present if the jet changes its shape within one acceleration regime, or if plasma bulk motion Lorentz factor saturates without a change in a jet boundary geometry. In all these cases the relation (13) must hold for a jump in measured core shift offset.

2. We discuss the different possible forms of a jump in core shift vs. observational frequency relations presented by the cartoons in Figure 1. We speculate, that the balance between a magnetic field and an emitting plasma energy density may change abruptly as a consequence of a

plasma acceleration at a shock or as a result of a reconnection event. This will also lead to a jump in $\Omega_{r\nu}$, given by Equation (14). If such an event takes place at the distances of a radio core at the frequencies 15–22 GHz, as expected in blazars possibly demonstrating a high-energy neutrino production (Plavin et al. 2020), it could be potentially detected by a dedicated search. Such events in general would produce a core shift offset jump that can be differentiated from the discussed thoroughly in this paper. If the break in a core shift appears due to plasma heating or a flare propagation, than the core shift exponent must be the same, and the value of a jump in general would not obey the relation (13).

3. Measuring both branches of a core shift offset allows limiting the parameter $\eta\Gamma_{\max}/\rho^2$ by using Equations (18) or (19). Thus, the detection of a core shift break refines a magnetic field estimate in the parabolic part of a jet. The latter may be extrapolated upstream the break and, possibly, onto the scales of a gravitational radius.

4. We have demonstrated on the example of NGC 315 how using both branches of a core shift may improve the precision of a magnetic field estimate. The break in a core shift together with a jet shape break can also refine estimation of the parameters of a jet geometry transition region.

5. Applying different cases of a relation between the observation angle and bulk motion Lorentz factor, we find that the case $\delta \approx 2\Gamma$ explains much better the rich observational data for NGC 315. However, it means that the observational angle of a jet must be of the order of 6° . Even for such small angle, the de-projected distance of a jet shape break lies well within the estimated Bondi sphere.

6. We propose the core shift break search as a possible new instrument for the location of a jet shape break in the larger sample of sources than available at the moment. The core shift measurements at high frequencies with the resolution provided by the space-ground interferometry will allow studying the jet acceleration regions even for high red shift sources.

ACKNOWLEDGEMENTS

We thank the anonymous referee for thoughtful comments and suggestions that helped to improve the paper. The work was supported by the Foundation for the Advancement of Theoretical Physics and Mathematics “BASIS”. This research made use of the data from the MOJAVE database¹ which is maintained by the MOJAVE team (Lister et al. 2018). This research made use of NASA’s Astrophysics Data System.

DATA AVAILABILITY

There is no new data associated with the results presented in the paper. All the previously published data has the proper references.

¹ <http://www.physics.purdue.edu/MOJAVE/>

REFERENCES

- Akiyama K., Asada K., Fish V., Nakamura M., Hada K., Nagai H., Lonsdale C., 2018, *Galaxies*, **6**, 15
- Asada K., Nakamura M., 2012, *ApJ*, **745**, L28
- Beskin V. S., Nokhrina E. E., 2006, *MNRAS*, **367**, 375
- Beskin V. S., Nokhrina E. E., 2009, *MNRAS*, **397**, 1486
- Beskin V., Chernoglazov A., Kiselev A., Nokhrina E., 2017, *MNRAS*, **472**, 3971
- Beskin V. S., Khalilov T. I., Nokhrina E. E., Pashchenko I. N., Kravchenko E. V., 2024, *MNRAS*, **528**, 6046
- Blandford R. D., Königl A., 1979, *ApJ*, **232**, 34
- Blandford R., Znajek R., 1977, *MNRAS*, **179**, 433
- Blandford R., Meier D., Readhead A., 2019, *Annual Review of Astronomy and Astrophysics*, **57**, 467
- Boccardi B., et al., 2021, *A&A*, **647**, A67
- Boizelle B. D., et al., 2021, *ApJ*, **908**, 19
- Bromberg O., Nakar E., Piran T., Sari R., 2011, *ApJ*, **740**, 100
- Chatterjee K., Liska M., Tchekhovskoy A., Markoff S. B., 2019, *MNRAS*, **490**, 2200
- Event Horizon Telescope Collaboration 2021, *The Astrophysical Journal Letters*, **910**, L13
- Frolova V., Nokhrina E., Pashchenko I., 2023, *MNRAS*, **523**, 887
- Hada K., Doi A., Kino M., Nagai H., Hagiwara Y., Kawaguchi N., 2011, *Nature*, **477**, 185
- Hada K., et al., 2018, *ApJ*, **860**, 141
- Hirota K., 2005, *ApJ*, **619**, 73
- Kino M., Takahashi M., Kawashima T., Park J., Hada K., Ro H., Cui Y., 2022, *ApJ*, **939**, 83
- Kino M., Ro H., Takahashi M., Kawashima T., Park J., Hada K., Cui Y., 2024, *ApJ*, **973**, 100
- Kirk J., Melrose D., Priest E., Benz A., Courvoisier T.-L., 1994, in *Saas-Fee Advanced Course 24: Plasma Astrophysics*.
- Komissarov S. S., Barkov M. V., Vlahakis N., Königl A., 2007, *MNRAS*, **380**, 51
- Komissarov S. S., Vlahakis N., Königl A., Barkov M. V., 2009, *MNRAS*, **394**, 1182
- Kovalev Y., Pushkarev A., Nokhrina E., Plavin A., Beskin V., Chernoglazov A., Lister M., Savolainen T., 2020, *MNRAS*, **495**, 3576
- Kudryavtseva N. A., Gabuzda D. C., Aller M. F., Aller H. D., 2011, *MNRAS*, p. 768
- Kutkin A. M., Pashchenko I. N., Sokolovsky K. V., Kovalev Y. Y., Aller M. F., Aller H. D., 2019, *MNRAS*, **486**, 430
- Levinson A., Globus N., 2017, *MNRAS*, **465**, 1608
- Lister M. L., Aller M. F., Aller H. D., Hodge M. A., Homan D. C., Kovalev Y. Y., Pushkarev A. B., Savolainen T., 2018, *ApJS*, **234**, 12
- Lister M. L., et al., 2019, *ApJ*, **874**, 43
- Lobanov A. P., 1998, *A&A*, **330**, 79
- Lyubarsky Y., 2009, *ApJ*, **698**, 1570
- Nakahara S., Doi A., Murata Y., Hada K., Nakamura M., Asada K., 2018, *ApJ*, **854**, 148
- Nakahara S., Doi A., Murata Y., Nakamura M., Hada K., Asada K., 2019, *ApJ*, **878**, 61
- Nakahara S., Doi A., Murata Y., Nakamura M., Hada K., Asada K., Sawada-Satoh S., Kamenoi S., 2020, *AJ*, **159**, 14
- Nakamura M., Asada K., Hada K., et al. 2018, *ApJ*, **898**, 146
- Nokhrina E., 2017, *MNRAS*, **468**, 2372
- Nokhrina E. E., Pushkarev A. B., 2024, *MNRAS*, **528**, 2523
- Nokhrina E. E., Gurvits L. I., Beskin V. S., Nakamura M., Asada K., Hada K., 2019, *MNRAS*, **489**, 1197
- Nokhrina E. E., Kovalev Y. Y., Pushkarev A. B., 2020, *MNRAS*, **498**, 2532
- Nokhrina E. E., Pashchenko I. N., Kutkin A. M., 2022, *MNRAS*, **509**, 1899
- Novikov I. D., Likhachev S. F., Shchekinov Y. A., Andrianov A. S., et al. 2021, *Physics - Uspekhi*, **64**, 386

- Okino H., Akiyama K., Asada K., Gómez J. L., et al. 2022, *ApJ*, **940**, 65
- Park J., Hada K., Nakamura M., Asada K., Zhao G., Kino M., 2021a, *ApJ*, **909**, 76
- Park J., Hada K., Nakamura M., Asada K., Zhao G., Kino M., 2021b, *ApJ*, **909**, 76
- Pjanka P., Zdziarski A. A., Sikora M., 2017, *MNRAS*, **465**, 3506
- Plavin A., Kovalev Y., Kovalev Y. A., Troitsky S., 2020, *ApJ*, **894**, 101
- Pushkarev A., Kovalev Y., Lister M., Savolainen T., 2009, *Astronomy & Astrophysics*, **507**, L33
- Pushkarev A. B., Hovatta T., Kovalev Y. Y., Lister M. L., Lobanov A. P., Savolainen T., Zensus J. A., 2012, *Astronomy & Astrophysics*, **545**, A113
- Pushkarev A. B., Kovalev Y. Y., Lister M. L., Savolainen T., 2017, *MNRAS*, **468**, 4992
- Ricci L., et al., 2022, *Astronomy & Astrophysics*, **664**, A166
- Ro H., Kino M., Sohn B., Hada K., Park J., Nakamura M., et. al. 2023, *Astronomy & Astrophysics*, **673**, 159
- Sironi L., Spitkovsky A., Arons J., 2013, *ApJ*, **771**, 54
- Sokolovsky K. V., Kovalev Y. Y., Pushkarev A. B., Lobanov A. P., 2011, *Astronomy & Astrophysics*, **532**, A38
- Tchekhovskoy A., McKinney J. C., Narayan R., 2009, *ApJ*, **699**, 1789
- Tomimatsu A., Takahashi M., 2003, *ApJ*, **592**, 321
- Tseng C.-Y., Asada K., Nakamura M., Pu H.-Y., Algaba J.-C., Lo W.-P., 2016, *ApJ*, **833**, 288
- Vlahakis N., 2004, *The Astrophysical Journal Letters*, **600**, 324
- Zamaninasab M., Clausen-Brown E., Savolainen T., Tchekhovskoy A., 2014, *Nature*, **510**, 126

This paper has been typeset from a $\text{\TeX}/\text{\LaTeX}$ file prepared by the author.